Hindawi
Journal of Nanomaterials
Volume 2017, Article ID 8275139, 9 pages
https://doi.org/10.1155/2017/8275139

Research Article

Electrical Impedance Measurements of PZT Nanofiber Sensors

Richard Galos,[1] Yong Shi,[1] Zhongjing Ren,[1] Liang Zhou,[2] Hao Sun,[1] Xiaoyu Su,[1] and Jianping Yuan[3]

[1]*Department of Mechanical Engineering, Stevens Institute of Technology, 1 Castle Point Terrace, Hoboken, NJ 07030, USA*
[2]*Department of Electrical and Computer Engineering, University of Florida, P.O. Box 116200, Gainesville, FL 32611-6200, USA*
[3]*National Key Laboratory of Aerospace Flight Dynamics, Northwestern Polytechnical University, 127 Youyu West Rd, Xi'an, Shaanxi Province 710072, China*

Correspondence should be addressed to Richard Galos; rgalos@stevens.edu

Received 21 October 2016; Accepted 15 December 2016; Published 29 January 2017

Academic Editor: Xiulin Fan

Electrical impedance measurements of PZT nanofiber sensors were performed using a variety of methods over a frequency spectrum ranging from DC to 1.8 GHz. The nanofibers formed by electrospinning with diameters ranging from 10 to 150 nm were collected and integrated into sensors using microfabrication techniques. Special matching circuits with ultrahigh input impedance were fabricated to produce low noise, measurable sensor outputs. Material properties including resistivity and dielectric constant are derived from the impedance measurements. The resulting material properties are also compared with those of individual nanofibers being tested using conductive AFM and Scanning Conductive Microscopy.

1. Introduction

The essential structures of nanomaterials at the nanoscale become altered to achieve desired properties, greatly extending their application and benefiting their usage. In our case, we leverage the very high specific surface area and high porosity of PZT nanofiber for enhanced piezoelectric output. This is ideal for sensor applications since this provides increased ability to acquire constituents and increased sensitivity to detect chemicals. Their smallness and lightness also result in fast response times. To produce sensing ability from nanofiber usually requires the embodiment of sensing material into the fibers [1] or coating [2, 3] them.

For our sensors, we mix a PZT sol gel with a precursor solution to impart piezoelectricity. Piezoelectric sensors are highly desirable since they produce electricity from environmental stimulus. They are used in a wide range of applications including momentary switches, impact and vibration sensors, accelerometers, strain gages, and imaging transducers. Although they are self-powered, they are typically integrated with amplifier and signal conditioning circuitry, depending on their particular use. Generally, they output signals (nanosensor) or harvest energy (nanogenerator). Either way, their output needs to be delivered to a load.

In order to obtain maximum power transfer from a device to a load, their impedance must be conjugately matched. Figure 1 represents a generalized connection of our device, having impedance Z_1 acting as a source and being connected to a load with impedance Z_2. As shown, a voltage divider circuit is formed between the source voltage, V_{source}, and the load voltage, V_{load}.

The ratio of the delivered load power to the source power, P_2/P_1, can be obtained by substituting each expression for V_{source} and V_{load} from Figure 1 into $P = V^2/Z$ and then calculating this power ratio. Noting R as the DC impedance, that is, imaginary parts vanish and complex Z becomes real R @ DC, we obtain

$$\frac{P_{\text{load}}}{P_{\text{source}}} = \frac{P_2}{P_1} = \frac{Z_2}{Z_1} \longrightarrow \frac{R_2}{R_1}\text{@DC}. \tag{1}$$

Proper characterization of nanomaterials is important to the device designer. By knowing the dielectric constant and adjusting device geometry, the capacitance of a device can be

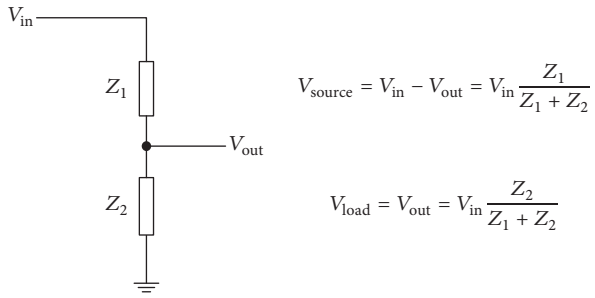

Figure 1: Voltage divider circuit representing generator with source impedance Z_1 and load impedance Z_2.

tailored to assist in impedance matching the device to interface circuitry at desired operating frequencies. PZT being a ceramic has inherently high electrical resistance. The resistivity of conductive nanofibers [4] has also been measured. Together with the tiny cross-sectional areas of nanodevices, extremely high DC resistances are encountered when more insulative materials are used like PZT, $BaTiO_3$, and PVDF.

There is much research of piezoelectric nanofiber devices reporting electrical outputs in many different ways. Generally, it is not always clear if the measured output is optimum under the given conditions and how the device output will vary over a range of different frequencies. For examples, Chen et al. [5] reported a PZT nanofiber generator output of 1.63 V and 0.03 μW. Wu et al. [6] reported a wearable PZT nanowire generator that could generate 6 V and 45 nA. Chang et al. [7] reported a single PVDF nanofiber generator that could generate 5–30 mV and 0.5–3 nA. Hansen et al. [8] used aligned PVDF nanofibers combined with a biofuel cell to power a UV sensor. Gu et al. [9] built a PZT nanowire array that produced an ultrahigh 209 V output with a current density of 23.5 $\mu A/cm^2$ s.

The impedance behavior of Si nanofibers was also studied by other researchers [10, 11] to understand electrochemical processes for use as anodes in lithium ion batteries. Capacitance of nanofibers [1] is also vital for supercapacitor applications.

2. Materials and Methods

2.1. Device Design and Fabrication. The nanogenerator device used for our measurements was developed at Stevens and is illustrated in Figure 2. Alternating pressure applied to the top surface of the polymer creates longitudinal mode stress of the PZT nanofibers resulting in charge generation. This induces a voltage difference between the two extraction electrodes.

The PZT nanofibers were made by an electrospinning process that used PZT sol gel in a precursor of ethanol and PVP. 10 kV was applied between the tip of the syringe and a high speed rotating grounded collector. Many layers of nanofibers accumulated forming a mat on top of a Si wafer attached to the collector. A sacrificial layer of MgO was deposited on the wafer beforehand using e-beam PVD. The wafers were then baked at 600°C to transition the PZT to a Perovskite phase. Interdigitated electrodes were added using

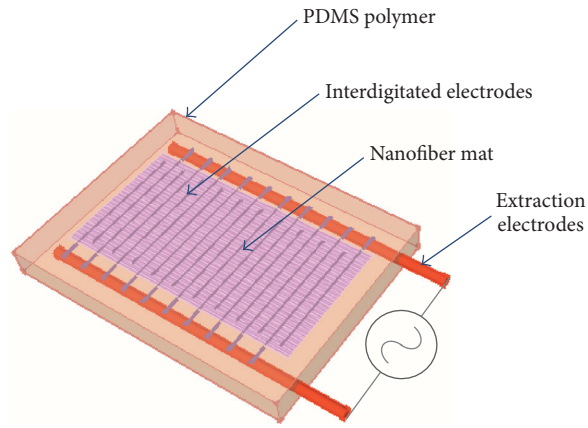

Figure 2: PZT nanogenerator developed at Stevens.

Table 1: Nanosensor used for Impedance Measurements along with Commercial reference.

	 Nanosensor	 Commercial*
Material	PZT nanofiber	PVDF film
Thickness	Avg 60 nm dia wire mesh	28 μm
Substrate	PDMS encapsulated	0.125 mm Polyester
Electrodes	50 μm dia Pt fine wire	Screen-print Ag-ink
Size	35 mm L × 20 mm W	25 mm L × 13 mm W

*see reference [12].

microfabrication techniques. Lastly, a PDMS polymer layer was applied.

For comparison and experimental measurement verification [13], a commercially available piezoelectric PVDF film sensor was also used. Photos and specifications of the sensors are shown in Table 1.

2.2. DC-IV Measurements. DC *I-V* characteristics of the sensor devices were measured with a Keithley 4200 SCS containing Source Measure Unit (SMU) modules equipped with a preamp. With this instrument, we simultaneously sourced the voltage and measured current. The additional preamp brought the current sensitivity down to 10 fA, which is similar performance to an electrometer picoammeter. All connections were guarded to reduce leakage currents and the devices were shielded within a metal enclosure to prevent electrostatic interference. Two-wire connections were used to connect with the DUTs. Although this connection introduced small lead resistance losses, they were negligible compared to the high resistance of our DUTs. (They would be more significant for low resistance DUTs.)

2.3. AC Impedance Measurements. AC impedance of the sensors was also measured with the same base SCS instrument using a built-in Capacitance Voltage Unit (CVU) module.

The coaxial leads were connected across the DUT inside a metal enclosure with a short jumper wire connecting the cable shields together. The frequency range spanned from 1 kHz to 10 MHz. Matlab™ was used to transform and operate on the C-V data.

To further extend the measurement frequency range from 1 MHz to 1.8 GHz, an Agilent 4291B Impedance Analyzer was used. The sample was mounted atop an adequate ground plane on a fixture that was calibrated out beforehand. This instrument measures impedance at a single port as the ratio of voltage to current. There are built-in impedance parameters to transform the data.

2.4. Superposition Method. A superposition method was conceived to estimate the PZT nanofiber dielectric constant from these impedance measurements. Specifically, in the process of fabricating a batch of sensors, we left some blank. Blank means that they contain no nanofibers, just the same electrode structure and PDMS encapsulation. We measured the impedance of both the full nanofiber sensors and the blank sensors (blank commercial sensors were not available). To obtain data for the nanofibers themselves, we subtracted the blank data from the full sensor data. Since the impedance is complex, subtraction of the corresponding real and imaginary components is carried out individually.

$$Z = R + jX. \tag{2}$$

Based on our interdigitated electrode arrangement, the whole sensor was treated as a parallel combination of individual "fingerlike" electrode pairs. For the real/resistive part, we solve for the nanofiber resistance as follows:

$$R_{\text{nano}} = \frac{R_{\text{eq}} R_{\text{blank}}}{R_{\text{blank}} - R_{\text{eq}}}. \tag{3}$$

With the resistive component of the nanofiber, R_{nano}, and knowing the sensor geometry, we find resistivity, ρ, by solving the following relation for ρ:

$$R = \frac{\rho L}{A}. \tag{4}$$

For our sensors, we used the electrode gap of 0.5 μm for L and the electrode length of 12 mm times the 100 nm average nanofiber diameter for the cross-sectional area, A.

Similarly, to find the dielectric constant of the PZT nanofiber mesh from the sensor and blanks, we first subtract the imaginary/capacitively reactive parts of the impedance:

$$X = \frac{1}{2\pi f C}. \tag{5}$$

The capacitance between individual electrodes is approximated based on the electrode geometry as illustrated in Figure 3. Our nanosensor configuration most closely resembles Figure 3(b) and is modeled accordingly, whereas Figure 3(a) is more representative of the commercial sensor.

Since capacitors in parallel add, $C_{\text{eq}} = C_{\text{nano}} + C_{\text{blank}}$, we solve for C_{nano} and then use these approximations to find the dielectric constant, ε_r. Here we use the electrode gap of 0.5 μm for a and eighteen times (for 9 electrode pairs) the 12 mm individual electrode length for the length, L.

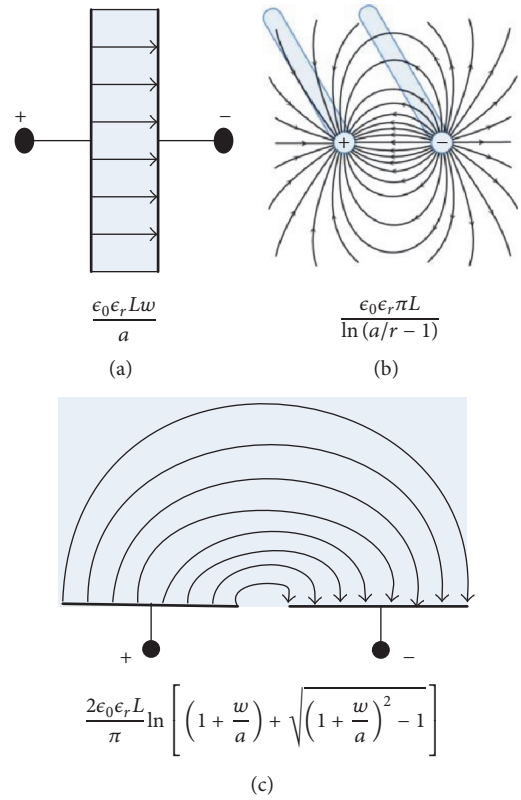

Figure 3: Approximations of capacitance for various electrode arrangements using a uniform dielectric material. Arrows indicate E-field (a) parallel flat plates with sandwiched dielectric, (b) parallel cylinders surrounded by dielectric, (c) coplanar with thick film dielectric.

Table 2: Estimated fractional power delivered to load from a generator having 50 TΩ DC source resistance.

Instrument	DC input impedance, R_2(MΩ)	Fractional power delivered, P_2/P_1
Oscilloscope	1	0.0000002
Lab amp	100	0.00002
Fabricated amp	50	1

2.5. Impedance Matching. For our ultrahigh source resistance nanosensors, ($R_1 \sim 50$ TΩ) we calculate, using (1), the expected power delivery using various instruments whose input impedance represents the load impedance and the results are shown in Table 2. Notice that a negligible amount of power is delivered when measuring with a typical oscilloscope having 1 MΩ input impedance. This result indicates that previous results [5] using a scope probe were questionable. In the process of trying to duplicate the previous results, we found that the measurements were highly susceptible to 60 Hz conducted emissions from AC power sources. It was at first difficult to realize; however, we found that disrupting noise could produce false signals. To remedy the 60 Hz noise, we utilized battery powered amplifiers and scopes.

In order to match our expected 50 TΩ impedance, we looked at several other laboratory instrument manufacturers

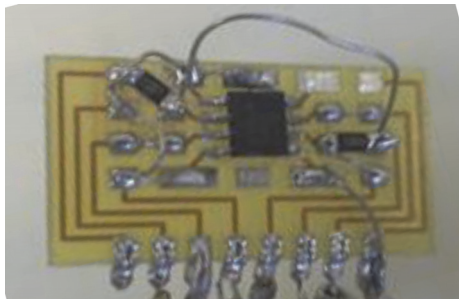

Figure 4: Unity gain voltage preamplifier built at Stevens from high input impedance DiFETs.

making preamplifiers for piezo applications; however they were all around a 100 MΩ value. Finally, we realized that we needed to build up our own preamplifiers starting from the component level and searched for discrete chips to match our targeted impedance value.

The latest technology from Texas Instruments highlighted a Dielectric FET (DiFET) that offered ultrahigh input impedance. This was about 3 orders of magnitude higher than other chips using Metal Oxide FETs (MOSFETs). The idea is that the dielectric insulated the gate of the transistor better than the metal oxide, requiring less field strength to operate. Three different circuits were then built and tested in our laboratory at Stevens using the same DiFET chip package. Figure 4 shows a voltage amp with unity gain (buffer) that was fabricated. We also made another amp with a gain of 10 as well as a charge amplifier.

Figure 5 shows a block diagram of the matched impedance measurement setup. Note that the nanogenerator DUT was shielded inside a metal enclosure to provide a Faraday cage which prevents susceptibility from any undesirable source of radiation that may be present in the environment. The leads to the amplifiers' input being guarded using a triaxial cable whose conductor adjacent to the signal contains the guard signal. All ground leads were kept short and tied to building ground to prevent ground loops.

We set up a test whereby a nanogenerator DUT was fixed at one end and deflected by hand using a long mechanical probe with a rounded tip. This is not exactly a DC excitation; however the deflection was applied slowly and steadily enough in an effort to produce piezoelectric charge at very low frequency such that very high impedance close to our DC approximation would exist.

Lastly, we characterized the sensor using this same matched impedance setup but with excitation from a mechanical shaker. We input certain frequencies away from known fixture resonances. For this experiment, a plastic cantilever beam was fixed rigidly at one end while the sensor was attached to the other free end. The shaker was driven sinusoidally using a function generator and amplifier.

2.6. Nanofiber Resistance Measurement. An Asylum Research MFP-3D Atomic Force Microscope (AFM) at Brookhaven National Laboratory was used to gather resistive data from individual nanofibers. The instruments' ORCA™ head with built-in function generator and op-amp readout circuitry provides a sample source voltage and produces a current map of the surface while operating in contact mode. Using this image, we pick certain "go to" measurement points that are atop of various nanofibers as well as appropriate void locations to subtract out the background noise. We were also able to obtain similar impedance data by applying an AC signal up to 5 kHz into the tip.

The samples that we prepared for this measurement consisted of individual nanofibers deposited on a Si wafer substrate. The substrate had a 5 nm Cr adhesion layer followed by a 100 nm Au layer applied to it ahead of time using a thermal deposition technique. Figure 6 illustrates the experimental setup that was utilized. The Au was needed to avoid oxidation during the baking of the nanofibers at 650°C which is part of the fabrication process. This provided adequate background contrast for our high resistance nanofibers.

Using this conductive AFM technique, we derived the impedance of our nanofiber samples by dividing the input voltage by the output current measured across the nanofiber diameter and into the conductive layer beneath our sample. Based on the nanofibers' diameter, the resistivity of the nanofibers was derived.

2.7. Nanofiber Capacitance Measurement. Our nanofiber capacitance measurement was also performed at Brookhaven National Lab using the same AFM. A Scanned Conductance Microscopy (SCM) technique was utilized that is able to detect the phase shift caused by a changing resonant frequency of the instruments' tip cantilever while scanning the sample. The cantilever tip encounters various tip to sample capacitances which change the electrostatic force on the tip that change the resonant frequency of the cantilever.

Samples of individual PZT nanofiber were deposited on top of a highly doped P-type Si substrate onto which a 10 nm layer of SiO_2 was thermally grown beforehand. Figure 7 illustrates the experimental setup that was utilized. A probe was connected to the edge of the sample where the SiO_2 layer was etched away with HF and coated with silver epoxy in order to form a contact point with the conductive Si substrate. Ground wires were connected from this contact point to equipment ground.

Once the AFM was set up, the topography was first learned in noncontact mode. This topographical surface calibration data was used to keep the AFM tip at constant scan height, h, above the sample (aka Lift Mode). Scan heights of 2, 5, and 10 nm were used. A DC voltage of 5 volts was applied from an internal source. Based on the nanofibers' diameter, the dielectric constant of the nanofibers was derived in a method similar to that of Hansen et al. [8] by using equations of motion of the cantilever beam system and the electrostatic forces acting.

3. Results and Discussion

3.1. DC-IV Measurements. The DC I-V characteristics of the devices are shown in Figure 8. As shown, the nanosensor resistances were between 50 and 100 TΩ, which is extremely high. The commercial device resistance, although still high,

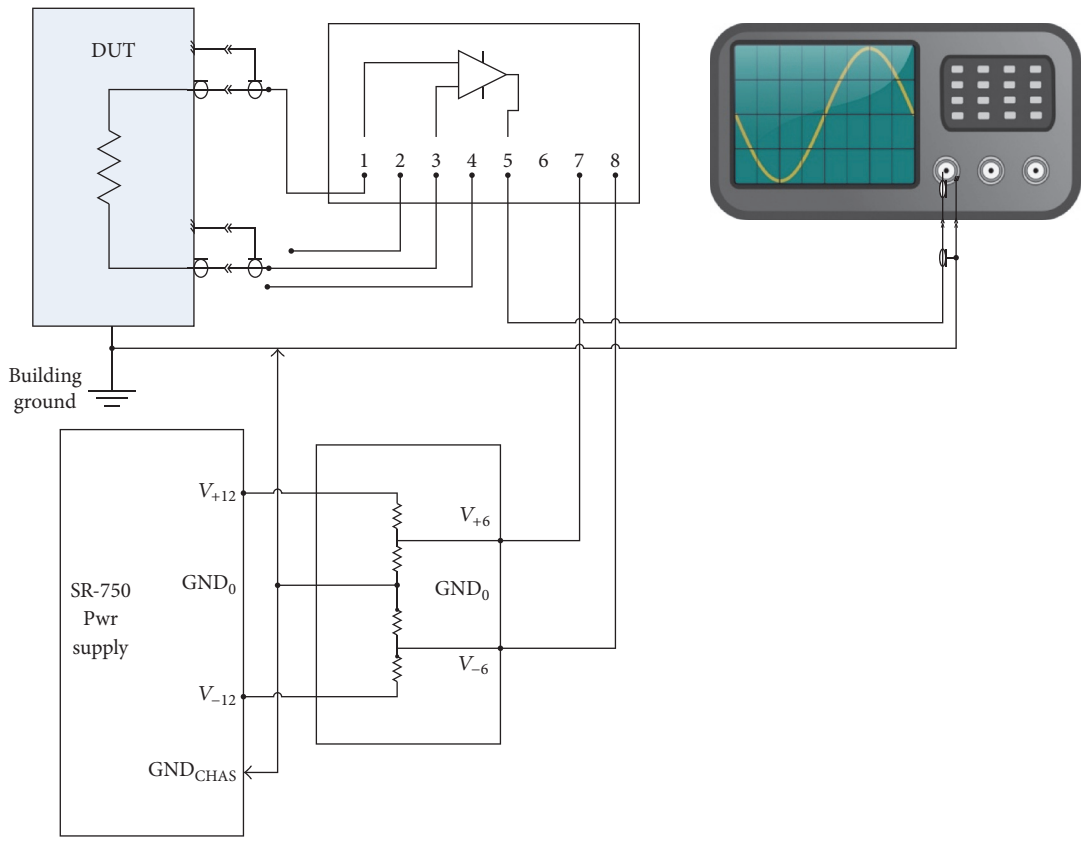

Figure 5: Block diagram of the matched impedance measurement setup.

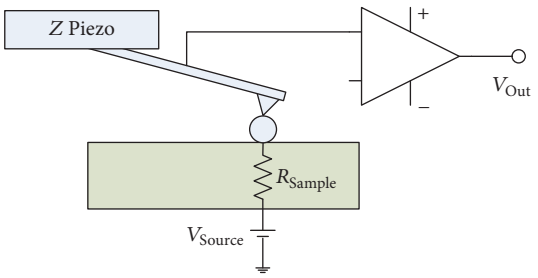

Figure 6: Block diagram of the nanofiber resistance measurement setup.

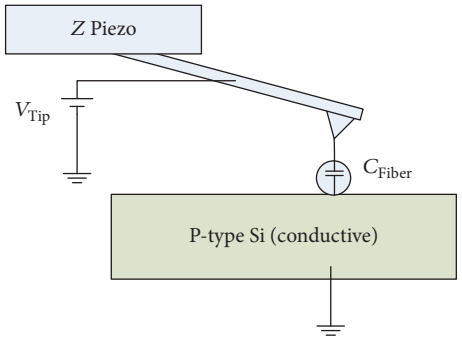

Figure 7: Block diagram of the nanofiber capacitance measurement setup.

was almost four orders of magnitude lower than the nanosensor.

3.2. AC Impedance Measurements. The resulting AC impedance of both the nanosensor and commercial sensor from 1 kHz to 10 MHz is shown in Figure 9. Notice how the impedances of both sensor types roll-off linearly (log-log scale) as a function of frequency. This is essentially a pure capacitive effect per (5). When we extrapolate down to about 10 Hz, we approach the DC resistance values that we measured from the previous DC *I-V* section. To get to 50 Ω (a practical impedance match), we need to extrapolate up to ~3 GHz for the nanosensor and to ~10 MHz for the commercial sensor.

Figure 10 shows a plot of the nanosensor impedance in an extended frequency range. Note that the first resonance peak (accompanied by a 90 degree phase shift) occurs just below 1 GHz. This is above the range of our previous SCS measurements. The trend out to 1.8 GHz shows impedance near 50 Ω.

3.3. Superposition Method. Figure 11 shows the nanofiber resistivity varying from about 10^5 down to 1 Ω-cm across the frequency band out to 10 MHz. Compared with bulk PZT [14] having a value of 1 GΩ-cm @ 100 Hz, the resistivity of

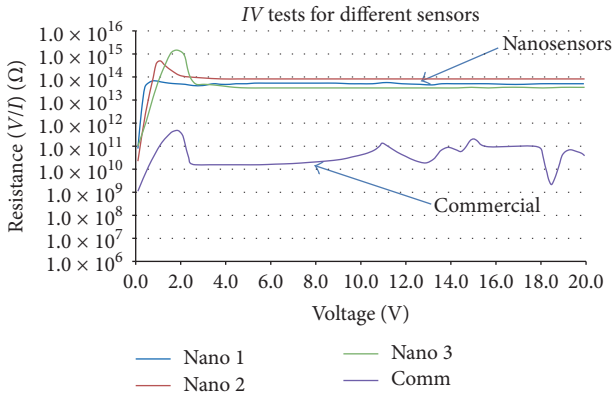

Figure 8: DC I-V characteristic of nanosensors and commercial sensor.

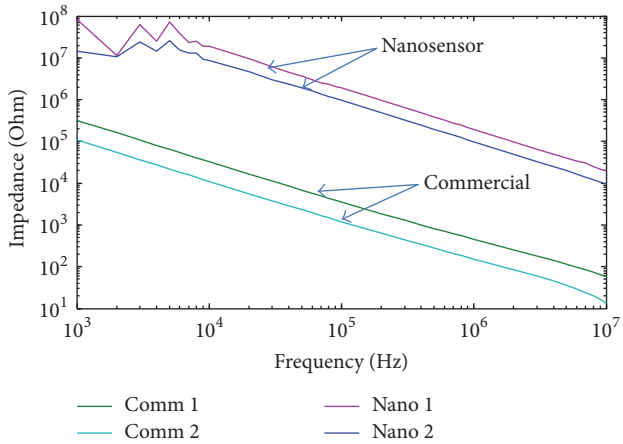

Figure 9: Impedance data for nanosensor and commercial sensor.

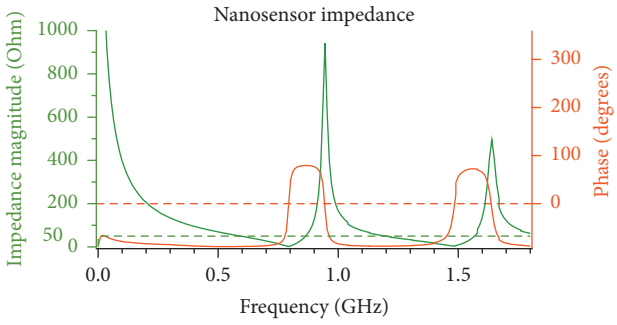

Figure 10: Nanosensor impedance measurement plotted over an extended frequency range, showing resonances.

the nanofiber mesh measured about 3 orders of magnitude lower and shows a similar but less dramatic decrease with increasing frequency.

Figure 12 shows that the nanofiber relative dielectric constant, ε_r, is between 350 and 600 (or 500 and 800 when extrapolated to 10 Hz) which is considerably smaller than bulk PZT whose $\varepsilon_r \sim 1300$. Comparatively, Zhu et al. [15] found the relative dielectric of ZnO nanofibers to shift down

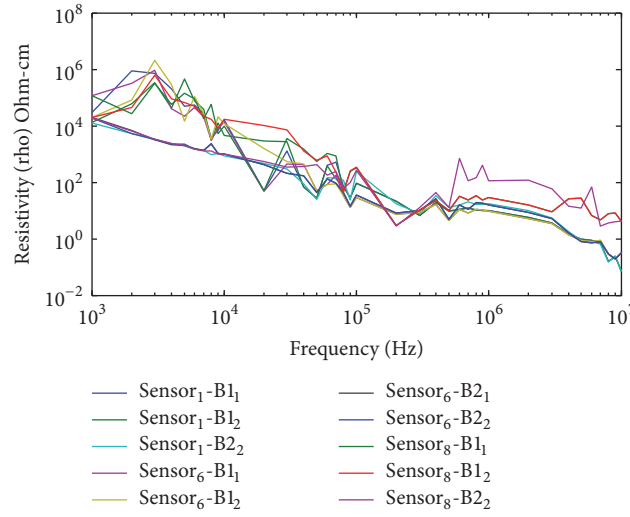

Figure 11: Nanofiber resistivity obtained by subtraction of real parts of (Sensor – Blank) impedance.

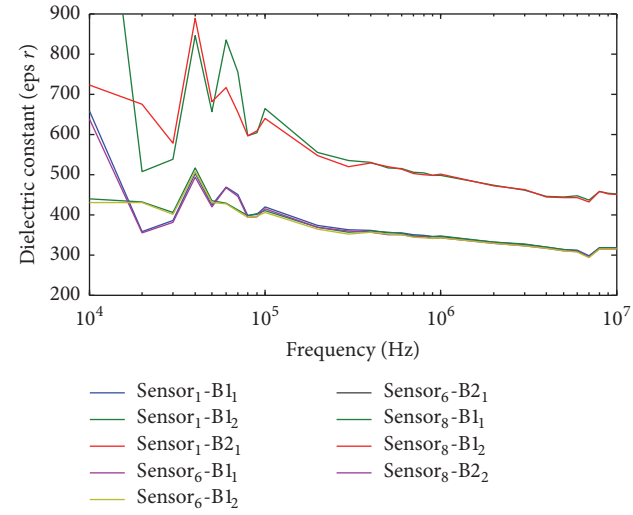

Figure 12: Nanofiber dielectric constant obtained by subtraction of imaginary parts of (Sensor – Blank) impedance.

from the bulk value of ~8.6 to the range of 6.4–2.7 at the nanoscale.

3.4. Impedance Matching. The 1 MΩ oscilloscope probe could not measure a discernible signal output signal from the nanogenerator. This was still the case with the probe switched to 10x for a 10 MΩ input impedance. We also tried a Stanford Research preamplifier having a 100 MΩ input impedance and a battery powered amplifier power feed. This lowered the noise floor to around 300 μV; however the signal to noise ratio was too low to identify a definite signal.

The resulting waveforms from our matched impedance measurement setup using manual excitation for both the nanogenerator and commercial sensor are shown in Figures 13(a) and 13(b), respectively. Notice that the noise floor was reduced to less than 0.1 mV and the signal to noise ratio is

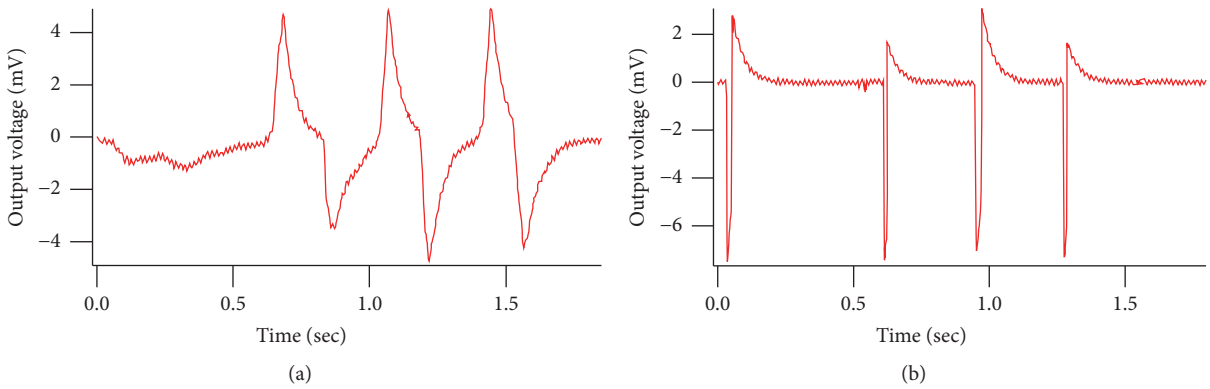

Figure 13: Output waveforms from matched impedance setup using manual excitation (a) nanosensor (b) and commercial reference sensor.

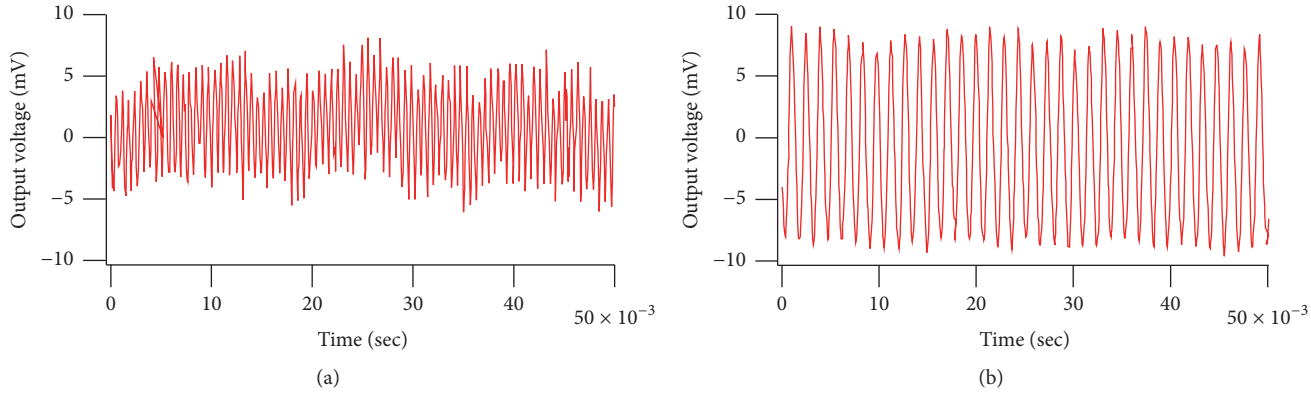

Figure 14: Output waveforms from matched impedance setup utilizing sinusoidal input from a mechanical shaker (a) nanosensor (b) and commercial reference sensor.

substantial. The commercial sensor output was expected to be lower than the nanosensor due to the mismatch; however it was slightly higher. We attribute this to the volume of piezoelectric material being much lower in the nanosensor.

Figure 14 shows the resulting waveforms from our matched impedance measurement setup using input from a mechanical shaker. A clean 18 mV pk-pk response @ 710 Hz with no fixture resonances was produced. Note that the nanogenerator did not produce a signal above the noise floor. This is partly because the PDMS polymer encapsulation was too thick. Our next generation of nanosensor presently being fabricated will have a very thin polymer coating that will reduce damping and provide improved adhesion between the sensor and the cantilever.

3.5. Nanofiber Resistance Measurements. Conductive AFM was performed on individual nanofibers as described and the results are compared against the sensor superposition method in Table 3.

3.6. Nanofiber Capacitance Measurements. The phase changes across many different size nanofibers were measured using the SCM method described and the resulting relative dielectric constants (ε_r) are plotted and fitted with a line as shown in Figure 15. To show how these results compare with the sensor superposition (impedance) method, data points in blue were added to the plot. Xu's previous results using the AAO template [16] is an additional point included in this figure. Additionally, the dotted line at the top of the figure shows the bulk value of 1300 for reference. As shown, the data from all 3 methods are reasonably close and the relative dielectric constant is a bit less than half the bulk value at 100 nm and varies approximately linearly down to about 180 @ 20 nm.

Table 3: Comparison of resistivity results between measurements.

Measurement	Resistivity (GΩ-cm)	Frequency (Hz)
Bulk	1	100
Sensor	105 to 1	1 k to 10 M
Conductive AFM	700 to 20	10 to 5 k

4. Conclusions

The higher output derived from using a nanomaterial like PZT nanofiber for sensors was further enhanced by matching the output of a nanosensor fabricated from nanofibers to its load. Additionally, our measurements of the resistivity and dielectric constant of PZT nanofiber at the nanoscale provide more accurate data for modeling of nanodevices that use PZT nanofiber.

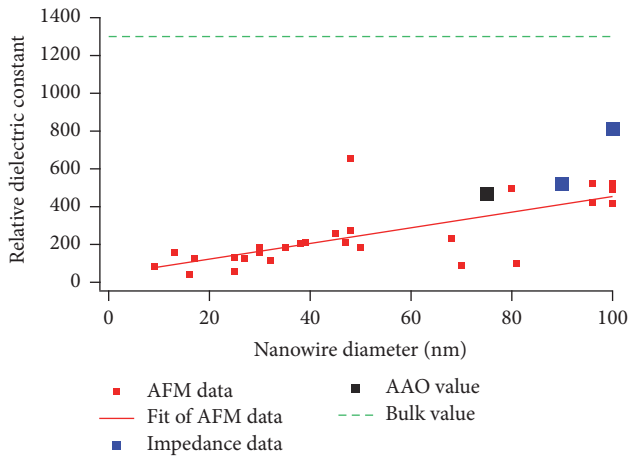

FIGURE 15: Results of various methods used to determine ε_r and comparison with bulk value.

PZT being a ceramic has inherently high electrical resistance. Together with the tiny cross-sectional areas of the PZT nanofiber mats in our nanosensors, extremely high DC resistances on the order of 100 TΩ resulted from our DC *I-V* measurements. Our AC impedance measurements that swept out to 1.8 GHz found that the sensors exhibited linearly decreasing impedance with frequency until resonances are encountered. To reach a common 50 Ω impedance match, it was extrapolated that our sensors would need to operate around 3 GHz. Overall, this shows the use of nanodevices to be more practical for power transfer at high frequency and how their capacitive reactance is relied upon to reduce their impedance for matching with practical circuits.

Improved sensor voltage output results were produced with lower noise than previously published measurements. This was accomplished by greatly reducing measurement noise and building ultrahigh input impedance amplifiers to match the device impedance for maximum power transfer.

A complex separation method was used to derive the resistivity and dielectric constant of PZT nanofiber with diameters ranging from 10 to 150 nm from sensor impedance measurements. From the results of these measurements, we estimate the resistivity of PZT nanofiber to be roughly three orders of magnitude less than the bulk value of ~1 GΩ-cm @100 Hz. Compared with bulk PZT the resistivity of the PZT nanosheet was 3 orders of magnitude lower and the dielectric constant was more than two times smaller at nanoscale.

Comparisons of the sensor impedance measurements with results from individual nanofiber measurements using an AFM were made. The resulting resistivity was within one order of magnitude to conductive AFM measurements of individual nanofibers. Likewise, the resulting dielectric constant was reasonably close to other individual fiber measurements using Scanning Conductance Microscopy.

Competing Interests

The authors declare that there is no conflict of interests regarding the publication of this paper.

Acknowledgments

The authors would like to acknowledge the assistance from other members of the Active Nanomaterials and Devices Laboratory at Stevens Institute of Technology including Guitao Zhang and Edward McGrath. Alltest Equipment, Farmingdale, NJ, was very supportive of our Impedance Analyzer measurements. The authors would like to thank Dymtro Nykypanchuk from Brookhaven National Laboratory for his helpfulness and support with AFM/SCM measurements.

References

[1] C. Kim and K. S. Yang, "Electrochemical properties of carbon nanofiber web as an electrode for supercapacitor prepared by electrospinning," *Applied Physics Letters*, vol. 83, no. 6, pp. 1216–1218, 2003.

[2] H. Niu, J. Zhang, Z. Xie, X. Wang, and T. Lin, "Preparation, structure and supercapacitance of bonded carbon nanofiber electrode materials," *Carbon*, vol. 49, no. 7, pp. 2380–2388, 2011.

[3] D.-Y. Youn, H. L. Tuller, T.-S. Hyun, D.-K. Choi, and I.-D. Kim, "Facile synthesis of highly conductive RuO2-Mn3O 4 composite nanofibers via electrospinning and their electrochemical properties," *Journal of the Electrochemical Society*, vol. 158, no. 8, pp. A970–A975, 2011.

[4] W. Gu and K. Kim, "A new approach to accurate resistivity measurement for a single nanowire—theory and application," in *Proceedings of the IEEE Nanotechnology Materials and Devices Conference (NMDC '06)*, pp. 304–305, IEEE, Gyeongju, South Korea, October 2006.

[5] X. Chen, S. Xu, N. Yao, and Y. Shi, "1.6 V nanogenerator for mechanical energy harvesting using PZT nanofibers," *Nano Letters*, vol. 10, no. 6, pp. 2133–2137, 2010.

[6] W. Wu, S. Bai, M. Yuan, Y. Qin, Z. L. Wang, and T. Jing, "Lead zirconate titanate nanowire textile nanogenerator for wearable energy-harvesting and self-powered devices," *ACS Nano*, vol. 6, no. 7, pp. 6231–6235, 2012.

[7] C. Chang, V. H. Tran, J. Wang, Y.-K. Fuh, and L. Lin, "Direct-write piezoelectric polymeric nanogenerator with high energy conversion efficiency," *Nano Letters*, vol. 10, no. 2, pp. 726–731, 2010.

[8] B. J. Hansen, Y. Liu, R. Yang, and Z. L. Wang, "Hybrid nanogenerator for concurrently harvesting biomechanical and biochemical energy," *ACS Nano*, vol. 4, no. 7, pp. 3647–3652, 2010.

[9] L. Gu, N. Cui, L. Cheng et al., "Flexible fiber nanogenerator with 209 V output voltage directly powers a light-emitting diode," *Nano Letters*, vol. 13, no. 1, pp. 91–94, 2013.

[10] R. Ruffo, S. S. Hong, C. K. Chan, R. A. Huggins, and Y. Cui, "Impedance analysis of silicon nanowire lithium ion battery anodes," *The Journal of Physical Chemistry C*, vol. 113, no. 26, pp. 11390–11398, 2009.

[11] A. R. Armstrong, G. Armstrong, J. Canales, and P. G. Bruce, "TiO2-B nanowires as negative electrodes for rechargeable lithium batteries," *Journal of Power Sources*, vol. 146, no. 1-2, pp. 501–506, 2005.

[12] Measurement Specialties, *Piezo Film Sensors Technical Manual*, P/N 1005663-1 REV E, 2008.

[13] R. Galos, Y. Xi, and S. Li, "Electrical impedance measurements of PZT nanofiber sensors," in *Proceedings of the ASME International Design Engineering Technical Conference IDETC/CIE*, Charlotte, NC, USA, August 2016.

[14] M. W. Hooker, "Properties of PZT-based piezoelectric ceramics between 150 and 250°C," Tech. Rep. NASA/CR-1998-208708, 1998.

[15] G. Zhu, R. Yang, S. Wang, and Z. L. Wang, "Flexible high-output nanogenerator based on lateral ZnO nanowire array," *Nano Letters*, vol. 10, no. 8, pp. 3151–3155, 2010.

[16] S. Xu and Y. Shi, "Power generation from piezoelectric lead zirconate titanate nanotubes," *Journal of Physics D: Applied Physics*, vol. 42, no. 8, Article ID 085301, 2009.